Surface Wind Variability on Spatial Scales from 1 to 1000 km Observed during TOGA COARE

CHRISTOPHER K. WIKLE, RALPH F. MILLIFF, AND WILLIAM G. LARGE

National Center for Atmospheric Research, Boulder, Colorado

(Manuscript received 5 December 1997, in final form 16 July 1998)

ABSTRACT

Near-surface wind spectra are considered from three very different data sources, covering a range of spatial scales from 10^0 to 10^3 km. The data were observed during the Tropical Ocean Global Atmosphere Coupled Ocean–Atmosphere Response Experiment intensive observation period spanning November 1992 to February 1993. Spectra are examined from low-resolution yet spatially and temporally complete National Centers for Environmental Prediction reanalysis wind fields, moderate resolution satellite-based *ERS-1* scatterometer winds, and high-resolution aircraft observations from the National Center for Atmospheric Research Electra. Combined spectra (kinetic energy vs wavenumber k) from these data demonstrate a power–law relation over the entire range in spatial scales, with a best-fit slope very near $k^{-5/3}$. Energy spectra for subsets of the data support spectral slopes of $k^{-5/3}$ and k^{-2}, but there is little evidence for a slope of k^{-3}.

1. Introduction

It is well known that there are multiscale interactions in tropical convective systems (e.g., Nakazawa 1988). Correspondingly, tropical wind systems are also dominated by multiscale interactions. Ideally, to examine the kinematic nature of such multiscale processes, one would like to examine the full joint space–time covariance structure suggested by the data. Equivalently, one could consider the space–time structure in the spectral domain. As a first step in this direction, we examine here the multiscale wavenumber spectra implied by a heterogeneous collection of surface wind data from the tropical Pacific. We compute near-surface wind spectra from three very different data sources, covering a range of spatial scales from 10^0 to 10^3 km. Specifically, we examine information from low-resolution ($\sim 10^2$ km) yet spatially and temporally complete analyzed wind fields, moderate-resolution ($\sim 10^1$ km) satellite-based scatterometer winds, and high-resolution aircraft observations ($\sim 10^0$ km). These observations were all taken during the Tropical Ocean Global Atmosphere Coupled Ocean–Atmosphere Response Experiment (TOGA COARE) intensive observation period (IOP) spanning November 1992 to February 1993 (Webster and Lukas 1992). As we will show, combined kinetic energy spectra from these data demonstrate a power-law relation with respect to (spatial) wavenumber k over more than three decades.

The power-law dependence of kinetic energy on spatial wavenumber invites comparison with power-law relations that arise from the classic theories for two- and three-dimensional turbulent flows [e.g., see reviews by Tennekes and Lumley (1972); Rose and Sulem (1978); Frisch (1995)]. According to the theories, nonlinear interactions between like-sized vortices (i.e., adjacent in wavenumber space) produce self-similar cascades of energy and enstrophy described by power laws across a range of scales. The energy and enstrophy flux directions (forward toward higher wavenumbers or inverse toward lower wavenumbers) and the spectral slopes that arise from the theories depend upon the dimensionality of the flow.

Kraichnan (1967), Batchelor (1969), and Lilly (1989) demonstrate the possible existence of two inertial subranges in two-dimensional turbulence. Numerical evidence for this concept is provided in calculations by Lilly (1969), as well as Maltrud and Vallis (1991). Approximate two-dimensionality is consistent with geophysical values for the stratification and rotation of the basic state in the atmosphere on planetary scales. Work in this regime by Charney (1971) on the theory of geostrophic turbulence demonstrates a forward enstrophy cascade. Work by Lilly (1983) relevant to atmospheric mesoscales, develops a ''quasi-two-dimensional'' approximation and demonstrates an inverse energy cascade. Conceptually, consider energy sources separated such that one source occurs at large scales (e.g., baroclinic instability of the large-scale flow) and the other at small scales (e.g., atmospheric convection). The

Corresponding author address: Dr. Christopher K. Wikle, 222 Math Sciences, University of Missouri, Columbia, MO 65211.
E-mail: wikle@stat.missouri.edu

quasi-two-dimensional theory suggests a forward enstrophy cascade at the largest scales with a spectral slope of k^{-3} and an inverse energy cascade with a spectral slope of $k^{-5/3}$ in the medium and small scales. A recent analytic demonstration of these cascades is provided by Lindborg (1999).

The quasi-two-dimensional approximation employed for the atmospheric mesoscale is not appropriate at submesoscale resolution [e.g., O(1 km)] where the flow is clearly three-dimensional. In the case of three-dimensional turbulence, a $k^{-5/3}$ energy spectrum can arise from a forward energy cascade (e.g., Rose and Sulem 1978; Frisch 1995). The analyses by Lindborg (1999) provide a means of identifying the scales at which the quasi-two-dimensional approximation breaks down.

In a competing interpretation outside turbulence theory, it has been argued that the interactions of a broadband population of atmospheric internal waves also give rise to a $k^{-5/3}$ mesoscale kinetic energy spectrum (Dewan 1979; VanZandt 1982). However, the large distance from the surface and strong stratification required to support a rich spectrum of internal waves weakens this interpretation in the present case of spectra for near-surface winds.

Observational analyses of large-scale velocity fields in the atmosphere have revealed spectral slopes of the kind mentioned above and tentative connections to the dynamics have been made (Freilich and Chelton 1986; Lilly 1989). In particular, examination of upper-level (9–13 km) wind fields from aircraft observations have proven enlightening (Gage 1979; Lilly and Petersen 1983; Nastrom and Gage 1983; Nastrom et al. 1984; Nastrom and Gage 1985; Gage and Nastrom 1986). More recent work by Lindborg (1999) discovers similar spectra from a new aircraft dataset similar to the data analyzed by Gage, Nastrom, and coworkers. Each of these studies found evidence of both the $k^{-5/3}$ slope at small scales and k^{-3} slope at larger scales. In between these regimes lies a transition region (10^2–10^3 km) where the spectral slope is less certain (e.g., Brown and Robinson 1979; Nastrom et al. 1984; Freilich and Chelton 1986). Bacmeister et al. (1996) examined midstratospheric velocity spectra over ranges from 100–1 km as obtained from high-altitude aircraft data. They found spectral slopes of approximately $k^{-2.5}$ for scales smaller than 6–12 km, and slopes of $k^{-1.5}$ to k^{-2} at scales longer than 12 km. As discussed by these authors, such results are inconsistent with any one turbulence theory. The authors interpret their results in a gravity wave context that is particularly plausible for the stratosphere.

Freilich and Chelton (1986) considered satellite-based scatterometer (Seasat) observations of the surface wind field and demonstrated an approximate k^{-2} slope for scales in the transition regime. They attribute the k^{-2} slope to a mixture of effects from the k^{-3} and $k^{-5/3}$ inertial subranges. They also find that the spectral slope of near-surface winds at these scales over the Tropics is slightly flatter than k^{-2}. They attribute this to the stronger convective sources in the Tropics relative to the baroclinic sources in the midlatitudes. It is not clear from the Freilich and Chelton (1986) study if the near-surface winds over the Tropics exhibit similar structure over a wider range of spatial scales. We address that question in this paper.

Numerical experiments have been designed to study turbulence properties of the atmospheric mesoscale, mostly in light of the spectra from aircraft observations (e.g., Bartello 1995; Vallis et al. 1997). Evidence for quasi-two-dimensional and separate cascades has been hard to establish in simulations in three dimensions. Stringent requirements for high spatial resolution, O(1 km), over large domains, O(1000 km), and integrations long enough to approximate realistic mesoscale equilibria constrain the interpretability of these efforts at present [for a summary see Lilly et al. (1998)]. Bartello (1995) employs a truncated set of Fourier modes to demonstrate that energy exchange from the vortical modes to gravity wave modes impedes an inverse energy cascade, even at scales where the two-dimensional approximation is appropriate. Conversely, Vallis et al. (1997) demonstrate approximate two-dimensionality, a $k^{-5/3}$ energy spectrum, and an inverse cascade in simulations representative of the atmospheric mesoscale, driven in part by convection. However, the authors point out that the effects of stratification, vertical shear, and boundary layer convergences and divergences that arise in these experiments depart from the assumptions consistent with the theory for two-dimensional turbulence.

In practice, with both observations and numerical experiments, it is difficult to identify precisely the ranges of wavenumber space over which two- or three-dimensional models for the flow field apply. Similarly, it is difficult to identify narrow bands of wavenumber space as energy sources and/or sinks that bound possible inertial subranges. One can distinguish the concept of ''stratified turbulence'' (K. S. Gage 1998, personal communication) from the dichotomy of two- versus three-dimensional turbulence as it is presented in the classic theories. In stratified turbulence, the flow is approximately two-dimensional in a layer-by-layer sense; however, the layers interact at small scales due to dissipative processes, and at larger scales under the influence of rotation. These ideas can be viewed as an extension to three dimensions of the quasi-two-dimensional turbulence concept introduced by Lilly (1983). Analytical work (e.g., Majda and Embid 1998) and numerical simulations (e.g., Vallis et al. 1997) in support of stratified turbulence concepts are in the formative stages at this time [see a multidisciplinary review in the compendium edited by Charbonneau et al. (1998)]. The 10-m winds we are about to analyze might also be considered in this context.

2. Data

We consider a region in the western Pacific Ocean basin covering 140°E to the date line, and 20°S–20°N,

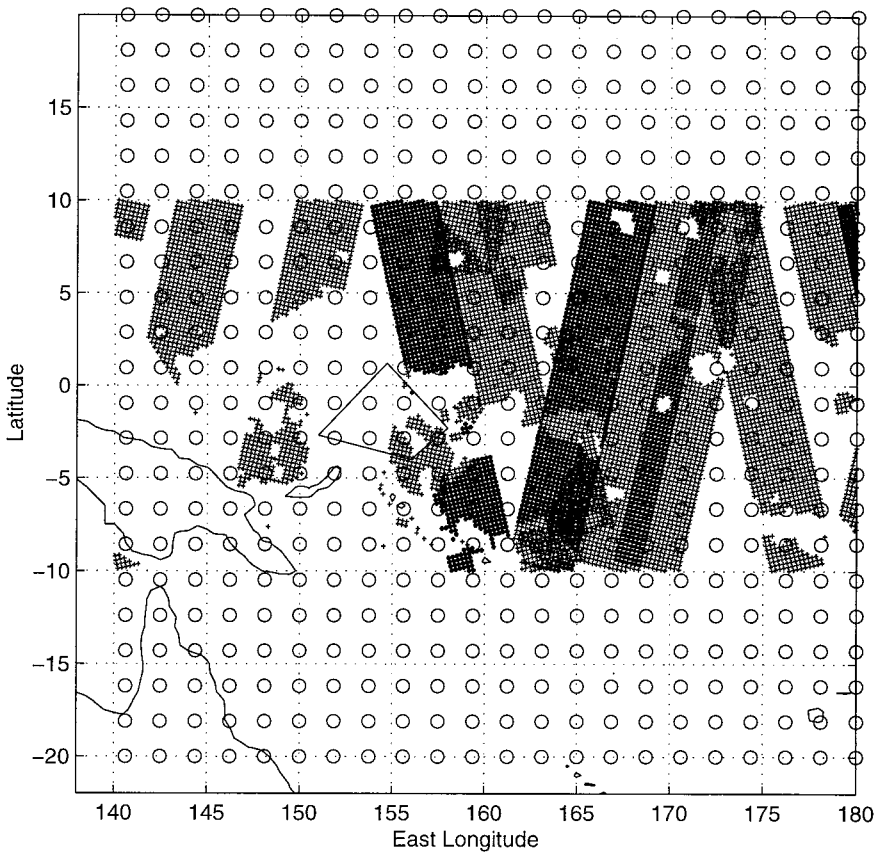

FIG. 1. Data locations. NCEP reanalysis locations (○) and *ERS-1* scatterometer observation locations (+) for days shown in Table 1. Note that the TOGA COARE IFA polygon is outlined as well.

as shown in Fig. 1. The largest spatial-scale dataset considered is the National Centers for Environmental Prediction (NCEP) reanalysis 10-m wind product, which has a reporting period of 6 h and spatial resolution of nearly 2°, or about 200 km (Gaussian grid transform from spectral truncation T62). The NCEP data occur at locations indicated by circles in Fig. 1. The information content of the reanalysis in this region concentrates on a much coarser spatial scale than the data that are reported. The NCEP winds should be thought of as numerical model results, that is, simulated winds, that are affected by observations in a way that is not easily determined for the region of our interest.

In addition to the NCEP reanalysis winds, we consider midscale resolution (25 km) near-surface wind estimates from the European Space Agency *European Remote Sensing Satellite* (*ERS-1*) scatterometer, as observed during the TOGA COARE IOP. Scatterometry is a technology whereby radar pulses emitted at specific frequencies and polarizations are backscattered by sea surface capillary waves (Attema 1991; Naderi et al. 1991). The backscattering is detected and related, through a ''geophysical model function,'' to surface stress and, ultimately, to a 10-m wind speed and direction (Freilich and Dunbar 1993; Stoffelen and Anderson 1997). The spatial scales characterizing these data are on the order of 50–500 km, while the temporal scales are uneven, with adjacent swath intervals on the order of hours and regional coverage on the order of days. The *ERS-1* scatterometer sampling for the tropical Pacific, during the TOGA COARE IOP, is described in Milliff et al. (1998). The sampling locations for the days used in our analysis [corresponding to the flight days of the National Center for Atmospheric Research (NCAR) Electra aircraft; see Table 1] are shown here in Fig. 1.

In addition to the NCEP reanalysis and *ERS-1* winds, we examine wind observations taken during 27 flights of the NCAR Electra aircraft during the IOP. We consider only data from flights with flight elevations between 30 and 40 m and with flight runs longer than 60 km. The data were averaged to give 1-km spatial resolution. A summary of the flights can be found in Table 1 of Sun et al. (1996). Since NCEP and *ERS-1* winds are from the 10-m level, the Electra data are interpolated to 10 m according to an equivalent neutral approximation for the atmospheric boundary layer (e.g., Liu and Tang 1996). This interpolation does not change sig-

TABLE 1. TOGA COARE IOP NCAR Electra flights used in spectral analysis.

Zonal		Meridional	
Day	Flight number	Day	Flight number
15 Nov 1992	1*, 2, 3, 4	28 Nov 1992	5, 6, 7
09 Dec 1992	12	09 Dec 1992	10, 11
10 Dec 1992	14	10 Dec 1992	13
09 Jan 1993	23, 24, 25	16 Dec 1992	17, 18, 19, 20, 21, 22
17 Jan 1993	27	14 Jan 1993	26

* Split into two series.

nificantly the spectral behavior relative to spectra that we examined using the winds as measured at the flight elevations. Neither the Electra data nor the *ERS-1* winds have been incorporated into the NCEP reanalysis dataset used in this study.

We are interested in wavenumber spectra for the zonal (u) and meridional (v) components of the near-surface wind sampled along approximately zonal and meridional tracks. In the case of NCEP reanalysis data, this approximation is exact. However, for scatterometer observations, zonal and meridional will refer to across track and along track, respectively. The deviations of the scatterometer sampling scheme from the zonal and meridional directions are not large in the Tropics (e.g., see Fig. 1) and the associated error in the spectral estimates is assumed to be negligible. Aircraft sample both components of the wind in the along-track direction only. Therefore, east–west flights of the NCAR Electra are used for zonal sampling while north–south flights are used for meridional sampling. Figure 2 shows the flight paths in the intensive flux array (IFA) and Table 1 shows our subjective classification into zonal and meridional flights.

To facilitate comparisons among datasets, we limit consideration of NCEP and *ERS-1* data to the same dates as the Electra flights. That is, meridional calculations were performed with NCEP and *ERS-1* data from the dates shown in the first column of Table 1, and similarly for the zonal direction. The total number of series used to calculate the spectra, as well as the approximate sampling interval and series length, are shown in Table 2.

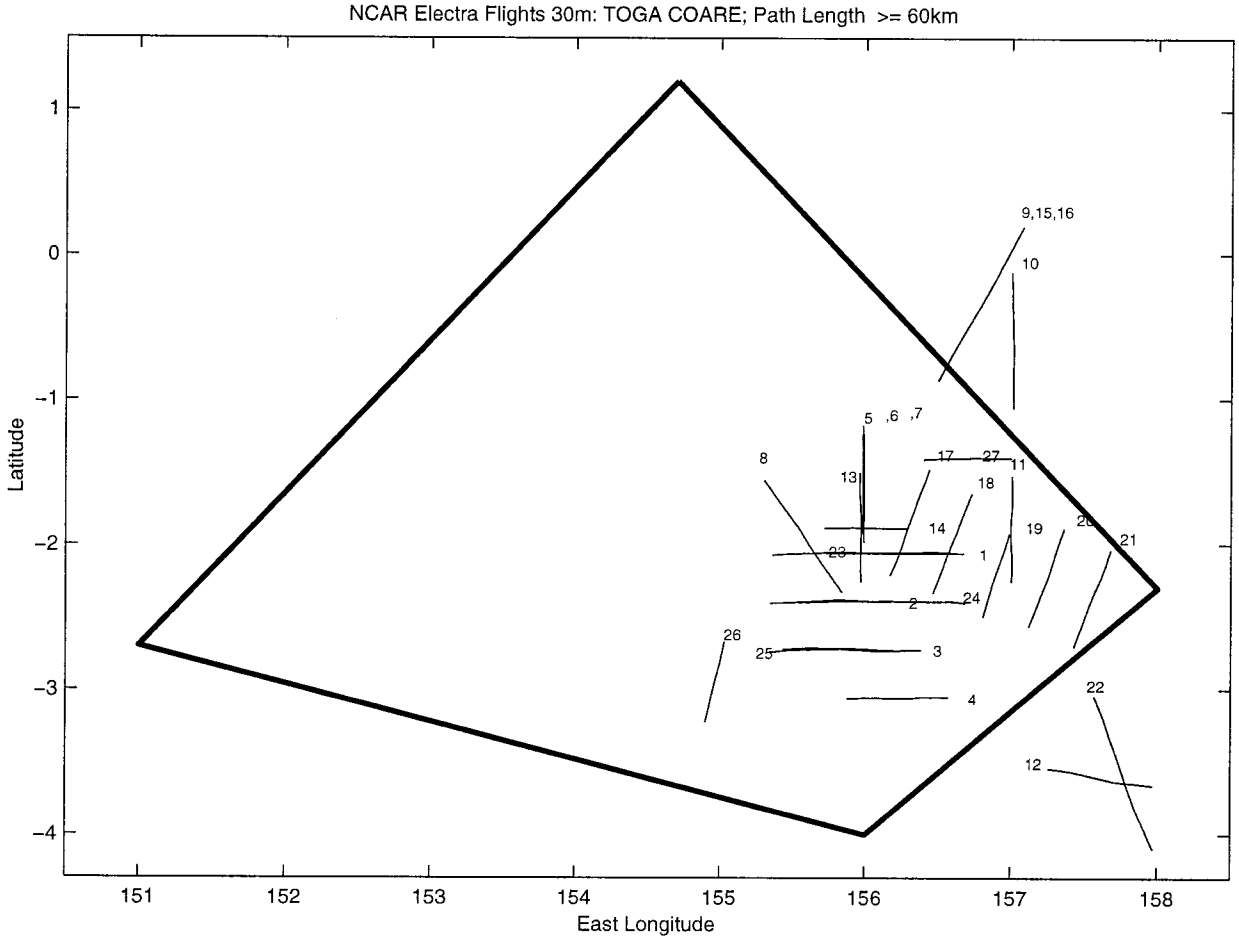

FIG. 2. TOGA COARE IFA region and flight paths of the NCAR Electra aircraft. Note that the flight paths chosen for analysis are presented in Table 1.

TABLE 2. Number of series, elements in each series, and approximate sampling interval for each dataset.

Dataset	Number of series		Number of elements		Approximate samp. int. (km)
	Zonal	Meridional	Zonal	Meridional	
NCEP	440	440	22	22	210
ERS-1	364	74	16	40	25
Electra	11	13	61	60	1

3. Analysis methods

The various wind datasets are analyzed independently to obtain estimates of wavenumber spectra. We estimate spectra following a Bartlett (1948) smoothing procedure wherein spectral estimates for several spatial series are averaged to gain a single statistically consistent spectral estimate.

We must take special care in the estimation of each individual spectrum since, in some cases, our series are very short (e.g., across-track scatterometer series have only 16 elements). For processes with a large dynamic range, the spectral estimate can be badly biased for wavenumbers at which the true spectrum is small (relative to other parts of the spectrum). This shifting of power between one portion of the spectrum and another is a function of the inherent windowing implied by the finite nature of the series and is known as spectral leakage. In our case, since wind spectra are typically red, we have a large dynamic range and power from lower wavenumbers can leak to higher wavenumbers, thus biasing the spectral estimates and inference regarding spectral slopes. One can decrease this bias by either tapering or prewhitening. Tapering is typically used in atmospheric applications (e.g., see Randel 1994) but is of little use with short series. Prewhitening (e.g., Percival and Walden 1993, 218–219) is a form of preprocessing that attempts to reduce the dynamic range of the series for which spectral estimates are desired. We choose a form of prewhitening in our analysis.

After removing potential linear trend from each spatial series, we employ an autoregressive (AR) prewhitening–postcoloring procedure as described in Percival and Walden (1993, 437–442). We first require an estimate of the first-order autoregression [AR(1)] parameter, which we obtain through lag-zero and lag-one autocovariance estimates based on the collection of series used for the Bartlett averaging. Estimation approaches for AR model parameters are discussed in most modern time series textbooks (e.g., Percival and Walden 1993, chap. 9). The estimated AR(1) parameter is used to create a filtered series. That is, assume we have a series X_s, for $s = 1, \ldots, N$. Then, given the AR(1) parameter estimate $\hat{\alpha}$, we obtain the filtered series $e_s = X_s - \hat{\alpha}X_{s-1}$, for $s = 2, \ldots, N$. This filtered series will then have smaller dynamic range than the original series, so we can estimate the spectrum of e_s with a traditional discrete Fourier transform spectral estimator. Then, since linear filtering theory gives a relationship between the spectrum of the AR(1) filter and its input (e_s) spectrum, and the output (X_s) spectrum, we can easily obtain the ''postcolored'' spectral estimate of X_s given the spectral estimate of e_s and the filter. Although not considered here, one can use more complicated filters in this procedure as well (Percival and Walden 1993, 438–439).

Since we obtain spectral estimates by averaging individual spectra from nearby geographical regions and times, our Bartlett averaged estimator is made up of a collection of correlated series. Due to the dependence introduced by such a collection, the variance of the Bartlett spectral estimate is necessarily a function of all the covariances between the individual spectral estimates. In practice, this makes the direct estimation of confidence intervals for the spectrum difficult. However, we can get reliable confidence intervals by considering a resampling approach that accounts for dependence between the spectra. In particular, we use the procedure for bootstrap confidence bands as described in Politis et al. (1992).

4. Results

Spectra and simultaneous 95% bootstrap confidence intervals for meridional velocities (v) sampled along zonal tracks, zonal velocities (u) along zonal tracks, meridional velocities along meridional tracks, and zonal velocities along meridional tracks are shown in Figs. 3a–d, respectively. The confidence intervals are a function of the number of series used in estimating the spectrum, which explains why there is relatively less confidence in the Electra spectral estimates. The first thing to note is that considering no normalization was employed, the spectra from the three different data sources match quite closely in amplitude (i.e., variance) for each case.

A persistent feature in Figs. 3a–d is the rapid drop of spectral power in the NCEP spectra from about 1000 km to the Nyquist scale (~400 km). This feature is consistent with what has been previously demonstrated to be the true wavenumber resolution of analysis data (Milliff et al. 1996). The rapid drop represents a departure from a power-law dependence with respect to wavenumber that could be due to the dissipation in the NCEP assimilation model and/or the effects of initialization. The high-wavenumber end of the NCEP spectra, corresponding to scales smaller than 900 km, were not included in estimates of the spectral slopes for the combined datasets (below). We note that the *ERS-1* slope matches the larger-scale part of the NCEP spectra quite well in each case (Figs. 3a–d). Similarly, the slopes tend to agree at the interface of the *ERS-1* Nyquist end (50 km) and the Electra large-scale end.

It is remarkable that the various velocity component–sampling direction pairings all demonstrate power-law dependencies of similar slopes. For an objective comparison of these power-law dependencies, we estimated

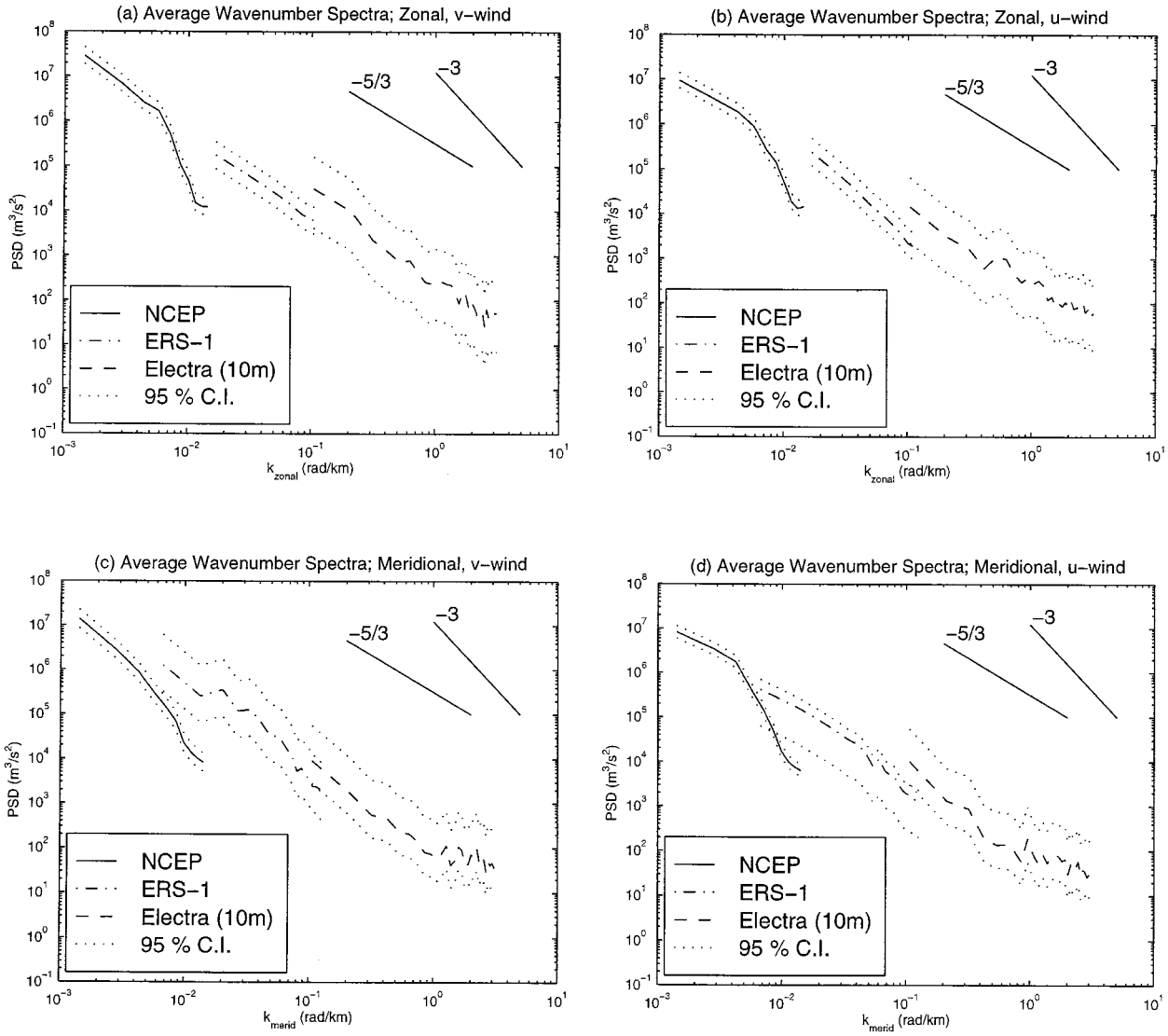

FIG. 3. Average wavenumber spectra and approximate 95% simultaneous bootstrap confidence intervals for NCEP, *ERS-1*, and NCAR Electra data for days when the Electra flew approximately zonal and meridional flight paths (Table 1); (a) zonal sampling of v wind, (b) zonal sampling of u wind, (c) meridional sampling of v wind, and (d) meridional sampling of u wind. The Electra data have been converted to 10 m by a neutral stability correction. Note that reference slopes of k^{-3} and $k^{-5/3}$ are shown for comparison.

the log–log slope and intercept associated with each dataset, wind component, and sampling track. Furthermore, estimates were obtained for various combinations of these datasets. The slope estimates and 95% confidence intervals are shown in Table 3. To obtain the values shown in Table 3, we employed a weighted least squares (WLS) estimation strategy, whereby the estimates of slope, intercept, and their standard errors reflect the relative precision of the various datasets. That is, each spectral estimate used in the regression is weighted by a measure of its precision (e.g., variance). This is accomplished by assuming that the error covariance matrix in the linear regression is diagonal (rather than the white-noise assumption in ordinary least squares regression), with diagonal elements proportional to the bootstrap 95% confidence intervals shown in Fig. 3. A discussion of WLS can be found in statistics textbooks concerned with regression analysis (e.g., Rawlings 1988, 315–318).

While small biases with respect to velocity component and sampling direction are evident for each dataset, in broad terms the spectral slopes shown in Table 3 are slightly steeper at lower wavenumbers (NCEP) and slightly flatter at the higher wavenumbers (Electra). As we can see from Table 3, the WLS estimate of the slope excluding unrealistic data from NCEP is between -1.61 and -1.69 at the 95% confidence level. The corresponding WLS linear fit and corresponding spectral es-

TABLE 3. Weighted-least-squares (WLS) estimates of log–log spectral slope and 95% confidence interval (C.I.).

Data	WLS slope	C.I.
Meridional, u wind		
NCEP (1–4)[a]	−1.97	[−4.01, 0.07]
ERS-1	−2.11	[−2.27, −1.94]
Electra[b]	−1.42	[−1.64, −1.20]
Electra (1–10)[c]	−2.05	[−2.62, −1.49]
Combined[d]	−1.67	[−1.73, −1.61]
Combined [Electra (1–10)][e]	−1.83	[−1.91, −1.75]
Zonal, v wind		
NCEP (1:4)	−2.09	[−2.37, −1.81]
ERS-1	−1.82	[−1.96, −1.68]
Electra	−1.90	[−2.05, −1.76]
Electra (1–10)	−2.20	[−2.48, −1.93]
Combined	−1.71	[−1.76, −1.66]
Combined [Electra (1–10)]	−1.77	[−1.87, −1.67]
Meridional, v wind		
NCEP(1:4)	−2.70	[−3.47, −1.92]
ERS-1	−2.38	[−2.68, −2.08]
Electra	−1.36	[−1.59, −1.14]
Electra (1–10)	−2.13	[−2.31, −1.96]
Combined	−1.65	[−1.73, −1.58]
Combined [Electra (1–10)]	−1.78	[−1.89, −1.67)
Zonal, u wind		
NCEP (1:4)	−1.65	[−2.24, −1.05]
ERS-1	−2.57	[−2.73, −2.41]
Electra	−1.55	[−1.68, −1.42]
Electra (1–10)	−1.61	[−1.98, −1.25]
Combined	−1.57	[−1.64, −1.50]
Combined [Electra (1–10)]	−1.67	[−1.81, −1.54]
M-u, Z-v (comb)[f]	−1.68	[−1.74, −1.63]
M-u, Z-v [comb; Elect (1–10)][g]	−1.80	[−1.89, −1.71]
M-v, Z-u (comb)[h]	−1.61	[−1.67, −1.56]
M-v, Z-u (comb; Elect (1–10)][i]	−1.73	[−1.81, −1.65]
M-u, Z-v, M-v, Z-u (comb)[j]	−1.65	[−1.69, −1.61]
M-u, Z-v, M-v, Z-u [comb; Elect (1–10)][k]	−1.77	[−1.83, −1.71]

[a] Only the first four NCEP spectral estimates were considered.
[b] All Electra data in this analysis were converted to 10 m under a neutral stability assumption.
[c] Only the first 10 Electra spectral estimates were considered.
[d] Includes NCEP (1–4), ERS-1, and ELECTRA data.
[e] Includes NCEP (1–4), ERS-1, and ELECTRA (1–10).
[f] Meridional u and zonal v wind data combined.
[g] Meridional u and zonal v wind data combined but with Electra (1–10).
[h] Meridional v and zonal u wind data combined.
[i] Meridional v and zonal u wind data combined but with Electra (1–10).
[j] Meridional u, v and zonal u, v wind data combined.
[k] Meridional u, v and zonal u, v wind data combined but with Electra (1–10).

timates are shown in Fig. 4. This slope is tantalizingly near a $k^{-5/3}$ power-law relation. A further subset of the data can be formed by reducing the number of Electra data to be more comparable with the numbers of *ERS-1* and NCEP data such that the WLS estimate of the spectral slope is not overly controlled by the Electra data. For this estimate, we only considered Electra data at spatial scales greater than approximately 5 km. The WLS estimate of the slope to the spectrum derived from this dataset is between −1.71 and −1.82 at the 95% confidence level (Table 3).

5. Discussion

As reviewed in the introduction, the overall $k^{-5/3}$ power-law relation evident in Fig. 4 might indicate 1) an inertial subrange and inverse energy cascade in two-dimensional turbulence, 2) an inertial subrange and forward energy cascade in three-dimensional turbulence, 3) some interaction of possibilities 1 and 2, or 4) none of the above (e.g., the internal wave mechanism described above).

While there is no evidence in our analyses at lowest wavenumbers for the k^{-3} dependence of Gage and Nastrom (1986), and the Electra data are perhaps too few to permit precise estimates of the spectral slope at highest wavenumbers, the slope of the combined spectra are remarkably similar to the prior observations from upper-level aircraft for scales of the order of 500 km and shorter. Not surprisingly, the kinetic energy amplitudes for the surface winds are about an order of magnitude smaller than the amplitudes for upper-level aircraft across the entire spectrum.

Gage and coworkers attribute the spectral slopes in their analyses to concepts of inertial subranges similar to the theory of quasi-two-dimensional turbulence. They suggest the possible existence of an energy sink at medium scales where the forward enstrophy cascade blends into an inverse energy cascade. However, Lindborg (1999) has shown that an energy sink in this range is not necessary for the transition between spectral slopes to occur. The dynamical regimes for surface winds in the Tropics, and for winds at elevations of convective outflow near the tropopause, are very different. However, we note that natural kinematic restrictions occur on the vertical velocities in each regime, making local two-dimensional approximations plausible in each place.

Our results concerning estimates of the spectral slopes roughly correspond to the scatterometer wind results of Freilich and Chelton (1986) for scales between 200 and 2000 km, wherein they measured a k^{-2} dependence in subtropical domains. Freilich and Chelton (1986) demonstrate that the power-law relations for velocity component spectra and kinetic energy spectra differ by a leading coefficient, but not in the spectral slope. Preliminary estimates of velocity component spectra from the later NASA Scatterometer (NSCAT) data demonstrate a shallowing of spectral slope as a function of latitude, with largest slopes ($\sim k^{-2}$) at high latitudes and shallowest slopes ($\sim k^{-5/3}$) at the equator (J. Morzel 1998, personal communication). The NSCAT record covers the period September 1996–June 1997. For a complete description of the NSCAT system see Naderi et al. (1991).

Conformity to the isotropic and nondivergence assumptions of two-dimensional turbulence theory can be

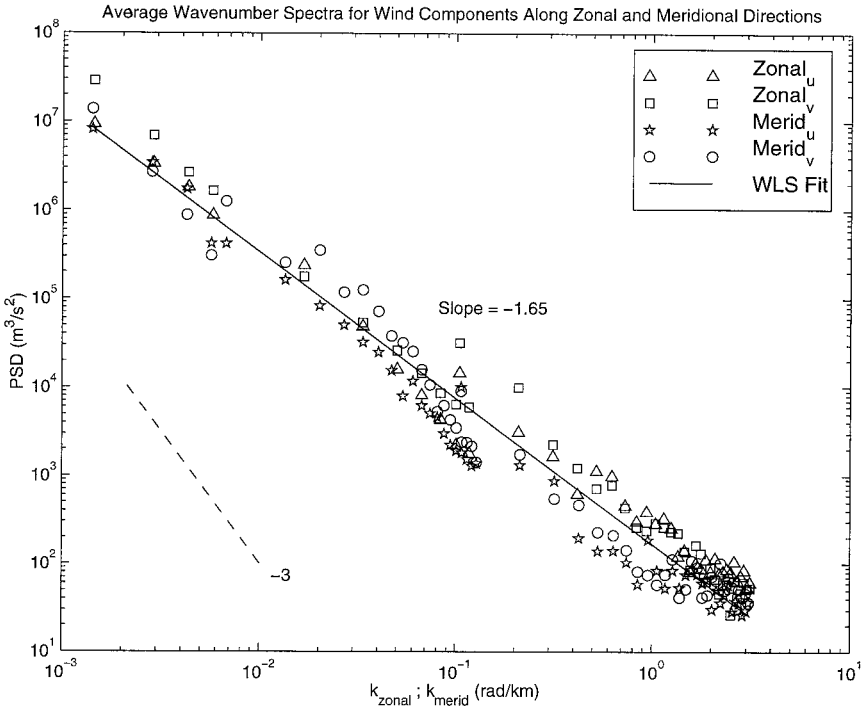

FIG. 4. Average wavenumber spectral estimates for u- and v-wind components for both zonal and meridional sample paths. Also shown is the WLS linear fit of these estimates. The regression is weighted by the relative precision of the spectral estimates. The dashed line depicts a k^{-3} spectral slope; a $k^{-5/3}$ slope is indistinguishable from the WLS fit of the data. Note that the NCEP data at higher wavenumbers have been excluded from the analysis as described in the text.

examined. Analyses of empirical covariance functions for the NCEP and *ERS-1* datasets suggest that the isotropy assumption is not valid. The zonal direction exhibits significant correlation at much longer spatial lags than does the meridional direction. As outlined in Freilich and Chelton (1986), the assumptions of isotropy and nondivergence can be tested by considering that the two-dimensional theory requires that the one-dimensional spectral power of the across-track component of the wind speed will be greater than the one-dimensional spectral power of the along-track component. That is, the ratio of the u wind variance to that of the v wind sampled along the meridional track should be greater than unity for isotropic, nondivergent flow. Similarly, the ratio of variances of the u wind to v wind sampled along the zonal track should be less than one. Examination of the variances for the zonal track in our case suggest that the ratio of u to v variability is indeed less than 1 for each dataset, supporting the idea of isotropic, nondivergent flow. However, for the meridional sampling track, the *ERS-1* ratio of u to v variance is also less than 1, suggesting in this case that the isotropic, nondivergent assumption is *not* valid, similar to the results in the subtropics of Freilich and Chelton (1986).

Lindborg (1999) develops a theory for distinguishing two- and three-dimensional flows and the respective cascades of enstrophy and energy. He finds the real-space structure functions to be more discerning of these properties than the Fourier-space spectra. The analyses of aircraft observations to demonstrate these methods (Lindborg 1999) benefit from a very large dataset, and therefore from well-converged results with respect to structure function behaviors. Our preliminary examinations of second- and third-order structure functions from the combined surface wind data for TOGA COARE demonstrate considerable scatter, suggesting that definitive results will require large and internally consistent datasets such as those obtainable from spaceborne scatterometer systems.

We note that there is a bias toward convectively inactive periods in the Electra sampling, as is usually the case for aircraft observations. Satellite and radar data for the time periods of the Electra flights during TOGA COARE (TCIPO 1993) demonstrated almost no aircraft sampling within regions of active convection inside the TOGA COARE IFA shown in Fig. 2. Although the NCEP and *ERS-1* spectral estimates were based on the data from the same days, the data used for the estimates covered a much broader geographical region than the IFA, thus including convective regions. Furthermore, spectral analysis of the NCEP and *ERS-1* data for the entire IOP (not shown) suggests similar results. Thus, the sampling bias evident in the Electra data does not affect our principal findings.

A strength and a limitation of the present analysis is the reliance on three very different data sources. It is a strength that such consistent results were obtained. However, each of these datasets has its own set of peculiarities related to sampling and measurement error bias. In fact, none of the three datasets used here consists of direct measurements of the surface wind speed. As we have described, the NCEP winds lack realistic variability at scales smaller than 1000 km. Moreover, there is mounting evidence in support of a conventional wisdom that finds the surface winds from NCEP to be too weak in strength and convergence in the Tropics. The *ERS-1* winds are derived empirically from measures of radar backscatter that are probably related more closely to surface wind stress. The Electra data are really space–time samples along a flight line that occurs at 30 m and higher, purposefully away from regions of active convection.

Such issues complicate the comparison and combination of these data. One tool that could be used to examine surface wind spectra more consistently would be a cloud-resolving model (CRM). Advances in computing technology have made it possible to examine long-time, large geographical extent two-dimensional (x, z) CRM solutions (e.g., Grabowski et al. 1996; Wu et al. 1998), as well as shorter-time and smaller-region three-dimensional CRM simulations (e.g., Wu and Moncrieff 1996). These models can provide the data necessary to evaluate the dimensionality, wavenumber spectra, and structure functions at various levels, under a variety of conditions, which can then be used to improve our understanding of observational results.

6. Conclusions

The kinematics of the near-surface wind field contain multiscale variability. Such data are critical for the proper forcing of oceanic GCMs (Large et al. 1991; Milliff et al. 1996). Thus, it is important to understand the spatial and temporal structure of near-surface winds. A first step in this regard is to investigate the wavenumber spectra of such data. Unfortunately, there are no unified datasets for the tropical oceans that cover the range of spatial and temporal scales necessary for such an analysis. However, we show that wavenumber spectra from three very different near-surface wind datasets (NCEP reanalysis, *ERS-1* scatterometer estimates, and Electra aircraft observations) over the TOGA COARE region suggest that an approximate $k^{-5/3}$ power law is evident over a large range in spatial scales (10^0–10^3 km). These results compare well with the $k^{-5/3}$ results in well-known spectra of upper-level aircraft data over a wavenumber range that is similarly broad. However, for the surface winds in the Tropics, we do not find evidence of a k^{-3} spectral slope at low wavenumbers.

Acknowledgments. Support for this research was provided for CKW by the NCAR Geophysical Statistics Project, sponsored by the National Science Foundation (NSF) under Grant DMS93-12686. Support for RFM and CKW is provided by the NCAR NSCAT Science Working Team cooperative agreement with NASA/JPL. We are grateful to Dr. Jielun Sun for providing the NCAR Electra data, to Mr. Jan Morzel for alerting us to recent results with NSCAT spectra, and to Dr. E. Lindborg for providing preprints of his recent work. We have benefited from three constructive reviews including comments from Dr. G. K. Vallis, and from discussions with Drs. K. S. Gage, R. M. Kerr, J. C. McWilliams, and J. J. Tribbia. NCAR is supported in part by the NSF.

REFERENCES

Attema, E. P. W., 1991: The active microwave instrument on board the ERS-1 satellite. *IEEE Proc.,* **79,** 791–799.

Bacmeister, J. T., and Coauthors, 1996: Stratospheric horizontal wavenumber spectra of winds, potential temperature, and atmospheric tracers observed by high-altitude aircraft. *J. Geophys. Res.,* **101,** 9441–9470.

Bartello, P., 1995: Geostrophic adjustment and inverse cascades in rotating stratified turbulence. *J. Atmos. Sci.,* **52,** 4410–4428.

Bartlett, M. S., 1948: Smoothing periodograms from time series with continuous spectra. *Nature,* **161,** 686–687.

Batchelor, G. K., 1969: Computation of the energy spectrum in homogeneous two-dimensional turbulence. *Phys. Fluids,* **12** (Suppl. II), 233–239.

Brown, P. S., and G. D. Robinson, 1979: The variance spectrum of tropospheric winds over eastern Europe. *J. Atmos. Sci.,* **36,** 270–286.

Charbonneau, P., J. R. Herring, and R. F. Milliff, 1998: Preface: Stratified, rotating turbulence. *Theor. Comput. Fluid Dyn.,* **11,** 135–136.

Charney, J. G., 1971: Geostrophic turbulence. *J. Atmos. Sci.,* **28,** 1087–1095.

Dewan, E. M., 1979: Stratospheric wave spectra resembling turbulence. *Science,* **204,** 832–835.

Freilich, M. H., and D. B. Chelton, 1986: Wavenumber spectra of Pacific winds measured by the Seasat scatterometer. *J. Phys. Oceanogr.,* **16,** 741–757.

——, and R. S. Dunbar, 1993: A preliminary C-band scatterometer model function for the ERS-1 AMI instrument. *Proc. First ERS-1 Symp., ESA SP-359,* Cannes, France, European Space Agency, 79–83.

Frisch, U., 1995: *Turbulence: The Legacy of A. N. Kolmogorov.* Cambridge University Press, 296 pp.

Gage, K. S., 1979: Evidence for a $k^{-5/3}$ law inertial range in mesoscale two-dimensional turbulence. *J. Atmos. Sci.,* **36,** 1950–1954.

——, and G. D. Nastrom, 1986: Theoretical interpretation of atmospheric wavenumber spectra of wind and temperature observed by commercial aircraft during GASP. *J. Atmos. Sci.,* **43,** 729–740.

Grabowski, W. W., X. Wu, and M. W. Moncrieff, 1996: Cloud-resolving modeling of tropical cloud systems during phase III of GATE, Part I: Two-dimensional experiments. *J. Atmos. Sci.,* **53,** 3684–3709.

Kraichnan, R. H., 1967: Inertial subranges in two-dimensional turbulence. *Phys. Fluids,* **10,** 1417–1423.

Large, W. G., W. R. Holland, and J. C. Evans, 1991: Quasi-geostrophic ocean response to real wind forcing: The effects of temporal smoothing. *J. Phys. Oceanogr.,* **21,** 998–1017.

Lilly, D. K., 1969: Numerical simulation of two-dimensional turbulence. *Phys. Fluids,* **12** (Suppl. II), 240–249.

——, 1983: Stratified turbulence and mesoscale variability of the atmosphere. *J. Atmos. Sci.,* **40,** 749–761.

——, 1989: Two-dimensional turbulence generated by energy sources at two scales. *J. Atmos. Sci.,* **46,** 2026–2030.
——, and E. L. Petersen, 1983: Aircraft measurements of atmospheric kinetic energy spectra. *Tellus,* **35A,** 379–382.
——, G. Basset, K. Droegemeier, and P. Bartello, 1998: Stratified turbulence in the atmospheric mesoscales. *Theor. Comput. Fluid Dyn.,* **11,** 137–152.
Lindborg, E., 1999: Can the atmospheric kinetic energy spectrum be explained by two-dimensional turbulence? *J. Fluid Mech.,* in press.
Liu, W. T., and W. Tang, 1996: Equivalent neutral wind. JPL Publication 96-17, 8 pp. [Available from the Jet Propulsion Laboratory, California Institute of Technology, Pasadena, CA 91109.]
Majda, A., and P. Embid, 1998: Averaging over fast gravity waves for geophysical flows with unbalanced initial data. *Theor. Comput. Fluid Dyn.,* **11,** 153–168.
Maltrud, M. E., and G. K. Vallis, 1991: Energy spectra and coherent structures in forced two-dimensional and beta-plane turbulence. *J. Fluid Mech.,* **228,** 321–342.
Milliff, R. F., W. G. Large, W. R. Holland, and J. C. McWilliams, 1996: The general circulation responses of high-resolution North Atlantic Ocean models to synthetic scatterometer winds. *J. Phys. Oceanogr.,* **26,** 1747–1768.
——, T. J. Hoar, and R. A. Madden, 1998: Fast, eastward moving disturbances in the surface winds of the equatorial Pacific. *Tellus,* **50A,** 26–41.
Naderi, F. M., M. F. Freilich, and D. G. Long, 1991: Spaceborne radar measurement of wind velocity over the ocean—An overview of the NSCAT scatterometer system. *Proc. IEEE,* **79,** 850–866.
Nakazawa, T., 1988: Tropical super clusters within intraseasonal variations over the western Pacific. *J. Meteor. Soc. Japan,* **66,** 823–839.
Nastrom, G. D., and K. S. Gage, 1983: A first look at wavenumber spectra from GASP data. *Tellus,* **35A,** 383–388.
——, and K. S. Gage, 1985: A climatology of atmospheric wavenumber spectra of wind and temperature observed by commercial aircraft. *J. Atmos. Sci.,* **42,** 950–960.
——, ——, and W. H. Jasperson, 1984: Kinetic energy spectrum of large- and mesoscale processes. *Nature,* **310,** 36–38.
Percival, D. B., and A. T. Walden, 1993: *Spectral Analysis for Physical Applications: Multitaper and Conventional Univariate Techniques.* Cambridge University Press, 583 pp.
Politis, D. N., J. P. Romano, and T.-L. Lai, 1992: Bootstrap confidence bands for spectra and cross-spectra. *IEEE Trans. Signal Processing,* **40,** 1206–1215.
Randel, W. J., 1994: Filtering and data preprocessing for time series analysis. *Statistical Methods for Physical Science,* J. L. Stanford and S. B. Vardeman, Eds., Academic Press, 283–311.
Rawlings, J. O., 1988: *Applied Regression Analysis: A Research Tool.* Wadsworth and Brooks/Cole, 553 pp.
Rose, H. A., and P. L. Sulem, 1978: Fully developed turbulence and statistical mechanics. *J. Phys.,* **39,** 441–482.
Stoffelen, A., and D. Anderson, 1997: Scatterometer data interpretation: Measurement space and inversion. *J. Atmos. Oceanic Technol.,* **14,** 1298–1313.
Sun, J., J. F. Howell, S. K. Esbensen, L. Mahrt, C. M. Greb, R. Grossman, and M. A. LeMone, 1996: Scale dependence of air–sea fluxes over the western equatorial Pacific. *J. Atmos. Sci.,* **53,** 2997–3012.
TCIPO, 1993: TOGA COARE Intensive Observing Period Operations Summary. [Available from the TOGA COARE International Project Office, University Corporation for Atmospheric Research, P.O. Box 3000, Boulder, CO 80307-3000.]
Tennekes, H., and J. L. Lumley, 1972: *A First Course in Turbulence.* The MIT Press, 299 pp.
Vallis, G. K., G. J. Shutts, and M.E.B. Gray, 1997: Balanced mesoscale motion and stratified turbulence forced by convection. *Quart. J. Roy. Meteor. Soc.,* **123,** 1621–1652.
VanZandt, T. E., 1982: A universal spectrum of buoyancy waves in the atmosphere. *Geophys. Res. Lett.,* **9,** 575–578.
Webster, P. J., and R. Lukas, 1992: TOGA COARE: The Coupled Ocean–Atmosphere Response Experiment. *Bull Amer. Meteor. Soc.,* **73,** 1377–1416.
Wu, X., and M. W. Moncrieff, 1996: Recent progress on cloud-resolving modeling of TOGA COARE and GATE cloud systems. *Workshop Proc. New Insights and Approaches to Convective Parameterization,* Reading, United Kingdom, European Centre for Medium-Range Weather Forecasts, 128–156.
——, W. W. Grabowski, and M. W. Moncrieff, 1998: Long-term behavior of cloud systems in TOGA COARE and their interactions with radiative and surface processes. Part I: Two-dimensional modeling study. *J. Atmos. Sci.,* **55,** 2693–2714.